PERGAMON

Automatica 38 (2002) 1881–1893

automatica

www.elsevier.com/locate/automatica

Drive torque actuation in active surge control of centrifugal compressors ☆

Jan Tommy Gravdahl[a,*,1], Olav Egeland[a], Svein Ove Vatland[b]

[a] *Department of Engineering Cybernetics, Norwegian University of Science and Technology, N-7491 Trondheim, Norway*
[b] *ABB Corporate Research, Bergerveien 12, N-1375 Billingstad, Norway*

Received 3 May 2001; received in revised form 4 January 2002; accepted 5 June 2002

Abstract

A novel approach to active surge control is presented for a centrifugal compressor driven by an electrical motor. The main idea of the paper is to use the *drive itself* for surge control. This eliminates the need for additional actuators, and has the potential of energy efficient operation. It is shown that previous unstable operating points to the left of the surge line can be made globally exponentially stable by using the rotational speed of the motor as control. It is then shown that stability and exponential convergence to a set follows when the torque of the drive is considered to be the control input. The proposed method is simulated on a compressor model using an approximation of a real compression system.

Keywords: Active control; Centrifugal compressors; Exponentially stable; Actuators; Nonlinear control; Lyapunov methods

1. Background

Centrifugal compressors are widely used for the pressurization of fluids. Applications include turbocharging of internal combustion engines, air compression in gas turbines used in power plants and for aircraft and marine propulsion. Another important application is pressurization and transportation of gas in pipelines and in the process and chemical industries. Surge is an unstable operation mode of centrifugal compressors which occurs when the operating point of the compressor is to the left of the surge line, which is the stability limit in the compressor map. Surge has been a major problem for designers and users of compressors since the invention of the turbocompressor. The phenomenon itself and the mechanism behind it is was recognized as early as 1924 by Stodola (1924). Also, according to Whittle (1953) surge was a serious problem in designing centrifugal compressors for the first jet engines. One of the first attempts to model surge mathematically was made by Emmons, Pearson, and Grant (1955), and a dynamic model suitable for control design was developed by Greitzer (1976). A general overview over surge phenomena can be found in Greitzer (1981) or in textbooks like Cumpsty (1989).

The surge phenomenon is manifested as oscillations of the mass flow, the pressure rise and the rotational speed of the compressor. Surge is highly undesired, and can cause severe damage to the machine. Traditionally, surge has been avoided using surge avoidance schemes. An example of such a scheme may be found in Staroselsky and Ladin (1979), and other methods may be found in Nisenfeld (1982) and Botros and Henderson (1994). Surge avoidance schemes use various techniques to keep the operating point of the compressor away from the surge line. Typically, a surge control line is drawn at a specified distance from the surge line, and the surge avoidance scheme ensures that the operating point does not cross this line. Usually, a recycle line with a recycle valve is constructed around the compressor and used for actuation. This method works well, as has been proved by numerous installations. However, due to the presence of the surge margin, the method restricts the operating range of the machine, and achievable efficiency is limited.

☆ This paper was not presented at any IFAC meeting. This paper was recommended for publication in revised form by Associate Editor Zhihua Qu under the direction of Editor Hassan Khalil.

* Corresponding author. Tel.: +47-73594393; fax: +47-73594399.
E-mail addresses: tommy.gravdahl@itk.ntnu.no (J.T. Gravdahl), olav.egeland@itk.ntnu.no (O. Egeland), svein.vatland@no.abb.com (S.O. Vatland).

[1] This work was performed while the author was also at ABB Industri AS, Oslo, Norway.

0005-1098/02/$ - see front matter © 2002 Elsevier Science Ltd. All rights reserved.
PII: S0005-1098(02)00113-9

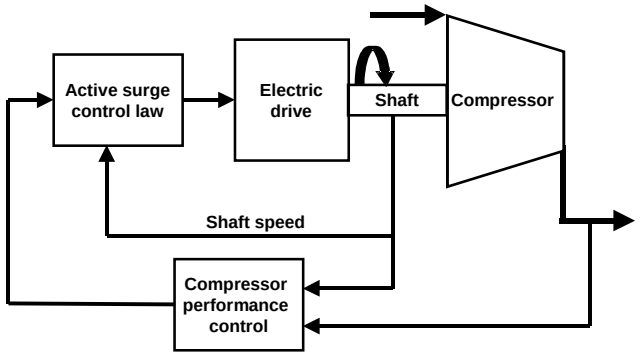

Fig. 1. The compression system consists of a centrifugal compressor driven by an electrical motor.

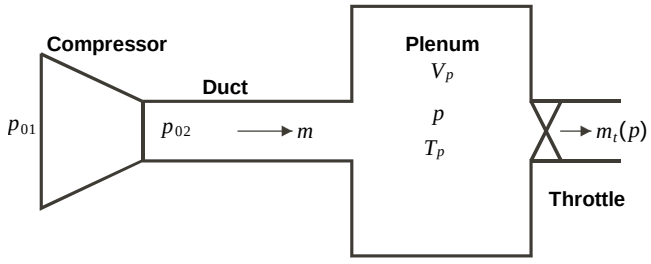

Fig. 2. The compressor, plenum, throttle system of Greitzer (1976).

Active surge control is fundamentally different to surge avoidance as unstable equilibria are sought to be stabilized instead of avoided. The motivation behind this is to overcome some of the shortcomings of surge avoidance. Active surge control of compressors was first introduced by Epstein, Williams, and Greitzer (1989), and since then a number of theoretical and experimental results have been published. Different actuators have been used, and examples include recycle valves, bleed valves and throttle valves, gas injection and variable guide vanes. For an overview, consult de Jager (1995), Gravdahl and Egeland (1999b) or Willems and De Jager (1999).

In this study, which is on compressors with electrical drives, we propose to use the electrical drive as a means of active surge control, as depicted in Fig. 1. The advantage of this is that the drive is already present, and no additional actuation device is required. This means that the compressor can be operated at a low flow without recycling, and there is a potential for reduced energy consumption of the compressor.

2. Model

2.1. Dynamics

A classical result in the field of compressor surge modeling is the model of Greitzer (1976) who modelled a basic compression system consisting of a compressor, a plenum volume, a throttle valve and in-between ducting as shown in Fig. 2. The model was derived by calculating the mass balance of the plenum volume, integrating the one-dimensional Euler equation (the momentum balance) over the length of the exit duct. In order to study the drive torque as a control variable for surge control, we need a model that takes variable speed into account. In Fink, Cumpsty, and Greitzer (1992), the Greitzer model was further developed, and rotational speed was included as a state in the model by calculating the torque balance of the rotating shaft. In Gravdahl and Egeland (1999a) the model was further developed, and a speed-dependent compressor characteristic was derived. The model is written

$$\dot{p} = \frac{a_{01}^2}{V_\mathrm{p}}(m - m_\mathrm{t}(p)), \tag{1a}$$

$$\dot{m} = \frac{A_1}{L_\mathrm{c}}(\Psi_\mathrm{c}(\omega, m)p_{01} - p), \tag{1b}$$

$$\dot{\omega} = \frac{1}{J}(\tau_\mathrm{d} - \tau_\mathrm{c}), \tag{1c}$$

where p is the plenum pressure, m is the compressor mass flow, ω is the rotational velocity, A_1 is the throughflow area, L_c is the duct length, V_p is the plenum volume, p_{01} and a_{01} are the inlet pressure and sonic velocity at ambient conditions, $m_\mathrm{t}(p)$ is the throttle flow, J is the sum of the inertia of the impeller, shaft and drive, τ_d is the drive torque, τ_c is the compressor load torque and $\Psi_\mathrm{c}(m, \omega)$ is the compressor characteristic, which will be presented in detail below. The mass flow through the throttle is given by

$$m_\mathrm{t}(p) = k_\mathrm{t}\sqrt{p - p_{01}} = k_\mathrm{t}\sqrt{p_{01}}\sqrt{\frac{p}{p_{01}} - 1}, \tag{2}$$

where the throttle parameter k_t is proportional to the valve opening. As in Gravdahl and Egeland (1999a), the compressor torque τ_c can be calculated as

$$\tau_\mathrm{c}(m, \omega) = \mu r_2^2 \omega m, \tag{3}$$

where r_2 is the impeller radius and μ will be defined in (11).

We will study stabilization and consider the dynamics around an equilibrium point. The equilibrium values are denoted by $(\cdot)_0$, while deviations from the equilibrium are denoted by $(\hat{\cdot})$. The deviations from the equilibrium are written as

$$\hat{m} = m - m_0, \tag{4a}$$

$$\hat{p} = p - p_0, \tag{4b}$$

$$\hat{\omega} = \omega - \omega_0, \tag{4c}$$

$$\hat{m}_\mathrm{t} = m_\mathrm{t} - m_{\mathrm{t}0}, \tag{4d}$$

$$\hat{\Psi}_\mathrm{c}(\hat{\omega}, \hat{m}) = \Psi_\mathrm{c}(\hat{\omega} + \omega_0, \hat{m} + m_0) - \Psi_{\mathrm{c}0}, \tag{4e}$$

where the equilibrium values must satisfy $m_0 = m_{\mathrm{t}0}$, $p_0 = \Psi_{\mathrm{c}0}$. Model (1) is transformed into the new coordinates (4) and

is then written as

$$\dot{\hat{p}} = \frac{a_{01}^2}{V_p}(\hat{m} - \hat{m}_t), \tag{5a}$$

$$\dot{\hat{m}} = \frac{A_1}{L_c}(\hat{\Psi}_c(\hat{\omega}, \hat{m})p_{01} - \hat{p}), \tag{5b}$$

$$\dot{\hat{\omega}} = \frac{1}{J}(\hat{\tau}_d - \hat{\tau}_c). \tag{5c}$$

For controller design we will first assume that control variable is the angular velocity ω of the compressor shaft. In that case we ignore the $\hat{\omega}$-dynamics, and the model is simplified to

$$\dot{\hat{p}} = \frac{a_{01}^2}{V_p}(\hat{m} - \hat{m}_t) \tag{6a}$$

$$\dot{\hat{m}} = \frac{A_1}{L_c}(\hat{\Psi}_c(\hat{\omega}, \hat{m})p_{01} - \hat{p}). \tag{6b}$$

Then, later, we will study the effect of the fact that the control variable is the electrical motor torque τ_d, while ω is controlled by an internal high gain loop.

2.2. Compressor characteristic

2.2.1. Derivation of the compressor characteristic

The compression process is modeled as an isentropic compression from p_{01} to p_{02} followed by an isobaric entropy increase. The change in stagnation enthalpy in the isentropic compression is denoted Δh_{0s}, while according to Ferguson (1963) the entropy increase is due to the shock loss Δh_{0i} related to incidence loss at the blade inlet and in the diffuser, and the fluid friction loss Δh_{0f}. The total increase Δh_{0t} of the stagnation enthalpy of the fluid contributed by the rotor is

$$\Delta h_{0t}(\omega, m) = \Delta h_{0s}(\omega, m) + \Delta h_{0i}(\omega, m) + \Delta h_{0f}(m).$$

The compressor characteristic is defined by

$$\Psi_c(\omega, m) = \frac{p_{02}}{p_{01}}.$$

Then, from the standard isentropic relations we get

$$\Psi_c(\omega, m) = \left(\frac{T_{0cs}}{T_{01}}\right)^{\kappa/(\kappa-1)} = \left(1 + \frac{\Delta h_{0s}}{c_p T_{01}}\right)^{\kappa/(\kappa-1)}, \tag{7}$$

where T_{0cs} is the stagnation temperature that would result at the rotor outlet if the compression from p_{01} to $\Psi_c p_{01}$ had been isentropic, and

$$\Delta h_{0s}(\omega, m) = \Delta h_{0t}(\omega, m) - \Delta h_{0i}(\omega, m) - \Delta h_{0f}(m). \tag{8}$$

Following Ferguson (1963), we assume the following expressions for the changes in stagnation enthalpy:

$$\Delta h_{0t} = \mu r_2^2 \omega^2, \tag{9a}$$

$$\Delta h_{0i} = \frac{r_1^2}{2}(\omega - \alpha m)^2, \tag{9b}$$

$$\Delta h_{0f} = k_f m^2. \tag{9c}$$

It is emphasized that the controller design and stability analysis presented below will still be valid for more elaborate expressions for the changes in stagnation enthalpy. In fact, the results that are presented are also valid for numerical approximations of the compressor characteristic $\Psi_c(\omega, m)$.

Combining (7)–(9), the following expression is found for the compressor characteristic:

$$\Psi_c(\omega, m) = \left(1 + \frac{\mu r_2^2 \omega^2 - \frac{r_1^2}{2}(\omega - \alpha m)^2 - k_f m^2}{c_p T_{01}}\right)^{\kappa/\kappa-1}. \tag{10}$$

Note that this expression is also valid in the unstable region to the left of the surge line. Here r_1 is the mean inducer radius, r_2 is the impeller radius, k_f is the fluid friction constant, T_{01} is the inlet stagnation temperature, c_p is the specific heat at constant pressure, c_v is the specific heat at constant volume and $\kappa = c_p/c_v$ is the ratio of specific heats. The constant $\alpha > 0$ determines the point of zero incidence loss, which occurs for $\omega - \alpha m = 0$. The constant is given by

$$\alpha = \frac{\cot\beta_{1b}}{\rho_1 A_1 r_1} = \frac{\omega_{surge\_line}}{m_{surge\_line}},$$

where β_{1b} is the inlet blade outlet angle and ρ_1 is the inlet density. The function

$$\mu = \sigma\left(1 - \frac{\cot\beta_{2b}}{\rho_1 A_1 r_1}\frac{m}{\omega}\right), \tag{11}$$

where β_{2b} is the rotor blade angle, accounts for rotor blades that are swept forwards or backwards. The function decreases with increasing mass flow for the usual backwards swept solution for blade design where $\beta_{2b} < 90^o$. The constant $\sigma = 1 - (n_{blades})^{-1}$ which is slightly less than unity, is the Stanitz slip factor, where n_{blades} is the number of blades.

2.2.2. Properties of the compressor characteristic

Now some properties of the compressor characteristic that will be of use in the following analysis will be presented. From expression (7) we find that the slope of the compressor characteristic $\Psi_c(\omega, m)$ with respect to the shaft velocity ω is given by

$$\frac{\partial\Psi_c}{\partial\omega} = \frac{\kappa}{\kappa-1}\left(\frac{T_{0cs}}{T_{01}}\right)^{1/(\kappa-1)}\frac{1}{c_p T_{01}}\frac{\partial h_{0s}}{\partial\omega} = \frac{\rho_d}{RT_{01}}\frac{\partial h_{0s}}{\partial\omega} = k_\rho\frac{\partial h_{0s}}{\partial\omega}, \tag{12}$$

where

$$\rho_d = \left(\frac{T_{0cs}}{T_{01}}\right)^{1/(\kappa-1)}\rho_{01}$$

is the density that would result at the rotor outlet if the compression from p_{01} to $\Psi_c p_{01}$ had been isentropic, and

$$k_\rho = \frac{\rho_d}{RT_{01}}$$

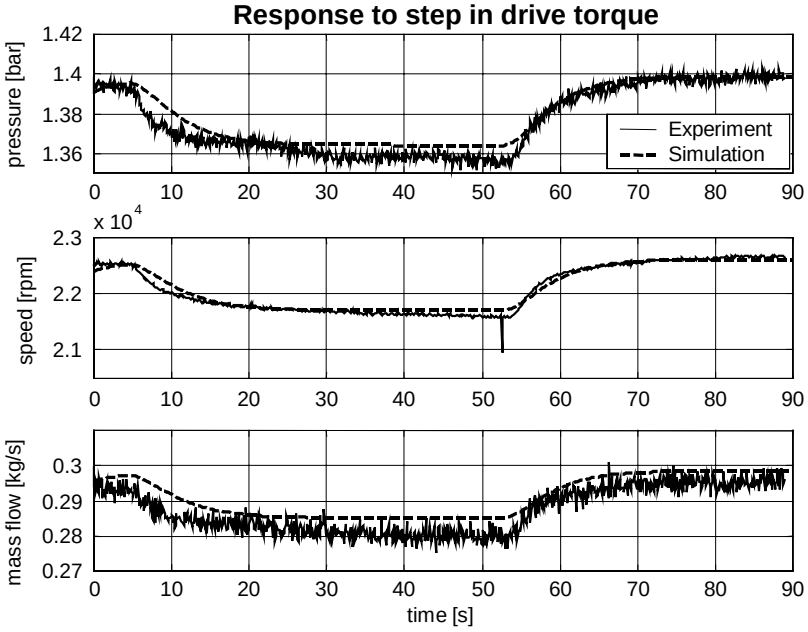

Fig. 3. Changing the set point by changing the drive torque. The fig. is taken from Gravdahl et al. (2002).

is a constant. By using the fact that $2\mu r_2^2 > r_1^2$, combining the derivative of (8) with respect to ω with (12), it is found that

$$g_\omega \triangleq \frac{\partial \Psi_c}{\partial \omega} = k_d(2\mu r_2^2\omega - r_1^2(\omega - \alpha m)) > 0. \tag{13}$$

This agrees with the well-known phenomenon that in centrifugal compressors the pressure ratio always increases with increasing shaft speed due to the centrifugal forces on the fluid. In a similar derivation as above, it is found that the slope of the compressor characteristic Ψ_c with respect to the mass flow m is

$$g_m \triangleq \frac{\partial \Psi_c}{\partial m} = \frac{\rho_d}{RT_{01}}\frac{\partial h_{0s}}{\partial m} = k_d\left(\frac{\partial h_{0t}}{\partial m} - \frac{\partial h_{0i}}{\partial m} - \frac{\partial h_{0f}}{\partial m}\right)$$
$$= k_d(r_1^2\alpha(\omega - \alpha m) - 2k_f m).$$

Define the surge line mass flow by

$$m_{sl}(\omega) \triangleq \frac{r_1^2\alpha}{r_1^2\alpha^2 + 2k_f}\omega.$$

Then $g_m < 0$ to the right of the surge line, that is for $m > m_{sl}$, and $g_m > 0$ to the left of the surge line, where $m < m_{sl}$.

2.3. Validation of the model

It is of great importance that the model (1) is accurate. Specifically, it is important that the effects of varying drive torque is captured as this is the basis for our control approach. Experimental results validating model (1a)–(1c) with compressor map (10), throttle flow (2) and compressor torque (3) were presented in Gravdahl, Willems, De Jager, and Egeland (2000) and Gravdahl, Willems, de Jager, and Egeland (2002). Simulations of both normal (transient) operation (see Fig. 3) and surge (see Fig. 4) were compared to experiments with very good results. The experiments were done at The Energy Technology Laboratory at Eindhoven University of Technology where a gas turbine installation has been build around a BBC VTR 160L turbocharger. The installation is described in Van Essen (1995).

3. Controller design

3.1. Surge control

The new feature of the proposed active surge control method is that we let the shaft velocity $\hat{\omega}$ be a function of the mass flow $\hat{m}$, thereby ensuring that the compressor can be operated to the left of the surge line without going into surge. We first assume that the shaft speed ω is our input control variable, and we will later consider the case that instead the drive torque τ_d is the control. The following theorem can now be stated:

The control law

$$\hat{\omega} = -c\hat{m}, \tag{14}$$

where the gain c is chosen according to

$$c > \frac{\partial \Psi_c/\partial m}{\partial \Psi_c/\partial \omega} = \frac{g_m}{g_\omega}$$

makes the origin of (6) globally exponentially stable.

Consider the Lyapunov function candidate

$$V(\hat{x}) = \frac{V_p}{2a_{01}^2}\hat{p}^2 + \frac{L}{2A}\hat{m}^2 > 0,$$

$$\forall \hat{x} = (\hat{m}\ \hat{p})^\top \neq (0\ 0)^\top. \tag{15}$$

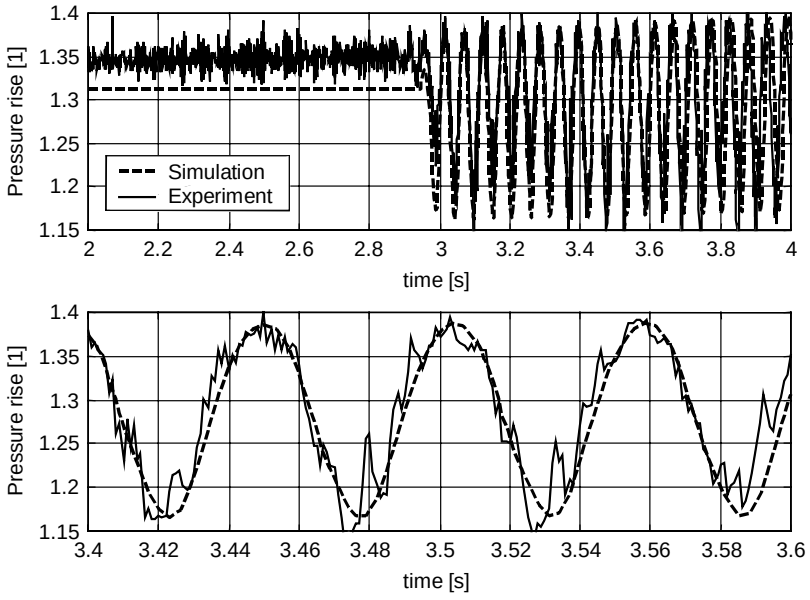

Fig. 4. Surge oscillations. The results from the simulation are close to the experimental values. The fig. is taken from Gravdahl et al. (2002).

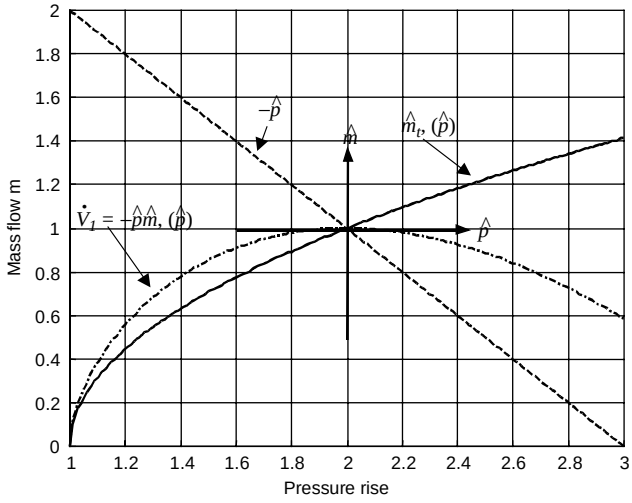

Fig. 5. Illustration of the calculation of $\dot{V}_1$. The derivative of the LFC is shown relative to the $(\hat{p}, \hat{m})$-system.

The time derivative along the solutions of (6) is

$$\dot{V} = \frac{a_{01}^2}{V_p}\,\hat{p}\dot{\hat{p}} + \frac{L}{A}\,\hat{m}\dot{\hat{m}} = \hat{p}(\hat{m} - \hat{m}_t) + \hat{m}(\hat{\Psi}_c p_{01} - \hat{p}).$$

This leads to the following expression for the time derivative:

$$\dot{V} = \dot{V}_1 + \dot{V}_2 = -\hat{p}\hat{m}_t(\hat{p}) + \hat{m}\hat{\Psi}_c(\hat{m}, \hat{\omega})\,p_{01}. \tag{16}$$

The throttle, or load, is assumed to be passive in the sense that it consumes energy from the compressor, which implies

$$\dot{V}_1 = -\hat{p}\hat{m}_t(\hat{p}) < -k_p\hat{p}^2 < 0, \quad \forall\,\hat{p} \neq 0 \tag{17}$$

for some $k_p > 0$, where k_p depends on the slope of the throttle characteristic. A plot of $\dot{V}_1$ is shown in Fig. 5.

In order to prove stability, we now proceed to show that $\dot{V}_2 = \hat{m}\hat{\Psi}_c(\hat{m}, \hat{\omega})\,p_{01} < 0$ when $\hat{\omega} = -c\hat{m}$. As $\hat{\Psi}_c(\hat{m}, -c\hat{m})|_{\hat{m}=0} = 0$, a sufficient condition for $\hat{\Psi}_c(\hat{m}, -c\hat{m})$ to be located in the 2nd and 4th quadrant in the $(\hat{m}, \hat{\Psi}_c)$-coordinate system is that $\hat{\Psi}_c(\hat{m}, \hat{\omega})|_{\hat{\omega}=-c\hat{m}}$ is monotonically *decreasing*, that is

$$\frac{d\hat{\Psi}_c(\hat{m}, \hat{\omega})}{d\hat{m}} = \frac{\partial\hat{\Psi}_c}{\partial\hat{m}} + \frac{\partial\hat{\Psi}_c}{\partial\hat{\omega}}\,\frac{\partial\hat{\omega}}{\partial\hat{m}} = \frac{\partial\hat{\Psi}_c}{\partial\hat{m}} - c\,\frac{\partial\hat{\Psi}_c}{\partial\hat{\omega}} < 0, \tag{18}$$

where (14) has been used. The condition (18) is satisfied provided c is chosen according to

$$c > \frac{\partial\hat{\Psi}_c/\partial\hat{m}}{\partial\hat{\Psi}_c/\partial\hat{\omega}} = \frac{\partial\Psi_c/\partial m}{\partial\Psi_c/\partial\omega} = \frac{g_m}{g_\omega},$$

where the first equality follows from the coordinate shifts (4a), (4c) and (4e). $\hat{\Psi}_c(\hat{m}, \hat{\omega})|_{\hat{\omega}=-c\hat{m}}$ is now monotonically decreasing and passing through the origin, that is located in the 2nd and 4th quadrants. Multiplying $\hat{\Psi}_c(\hat{m}, \hat{\omega})|_{\hat{\omega}=-c\hat{m}}$ with $\hat{m}$, which belong to the 1st and 3rd quadrants, then results in

$$\dot{V}_2 = \hat{m}\hat{\Psi}_c(\hat{m}, -c\hat{m})\,p_{01} < 0, \quad \forall\hat{m} \neq 0, \tag{19}$$

as is illustrated in Fig. 6. Moreover, $\dot{V}_2$ can always be bounded from above as

$$\dot{V}_2 = \hat{m}\hat{\Psi}_c(\hat{m}, -c\hat{m})\,p_{01} < -k_m\hat{m}^2, \quad \forall\hat{m} \neq 0. \tag{20}$$

for a constant $k_m > 0$. From (20) it follows that

$$\hat{\Psi}_c(\hat{m}, -c\hat{m})\,p_{01} < -k_m\hat{m}, \quad \hat{m} > 0. \tag{21}$$

As $\hat{\Psi}_c(\hat{m}, -c\hat{m})\,p_{01}$ is monotonically decreasing and passing through the origin, $\hat{\Psi}_c(\hat{m}, -c\hat{m})\,p_{01}$ is also bounded from

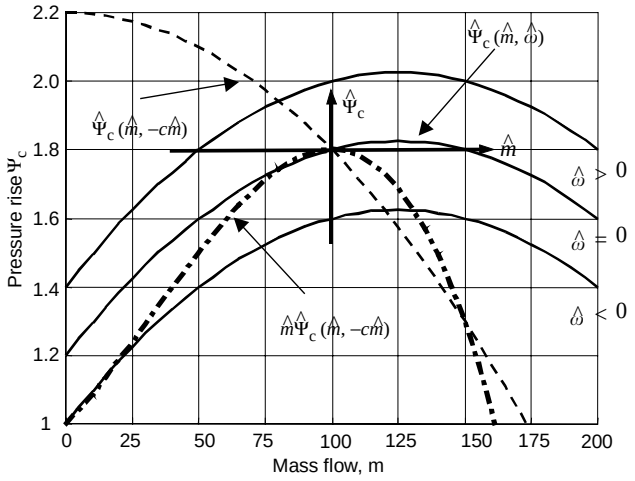

Fig. 6. Illustration of the calculation of $\dot{V}_2$. The time derivative of the LFC is shown relative to the $(\hat{m}, \hat{\Psi}_c)$-system.

above by the tangent through the origin, i.e.,

$$\hat{\Psi}_c(\hat{m}, -c\hat{m})\, p_{01} < p_{01} \frac{d\hat{\Psi}_c(\hat{m}, -c\hat{m})}{d\hat{m}} \hat{m}.$$

By choosing

$$k_m = -p_{01} \left. \frac{d\hat{\Psi}_c(\hat{m}, -c\hat{m})}{d\hat{m}} \right|_{\hat{m}=0}$$

(21) and (20) follows. A similar argument can be made for the case $\hat{m} < 0$. By (17), (20) and(15), we now have that

$$\dot{V} = \dot{V}_1 + \dot{V}_2 < -k_p \hat{p}^2 - k_m \hat{m}^2 < -kV, \quad \forall (\hat{m}, \hat{p}) \neq (0, 0),$$

where

$$k < \min \left\{ \frac{k_p}{V_p/2a_{01}^2}, \frac{k_m}{L/2A} \right\}$$

and the result follows.

Remark 1. It is seen from (14) that the gain c has a lower bound given by the ratio between the slope of the compressor characteristic $g_m = \partial \Psi_c / \partial m$, and the sensitivity of Ψ_c with respect to the shaft speed ω. This result is related to other results in active surge control for constant speed compressors, e.g.:

- When using the throttle valve for active surge control, Krstić, Protz, Paduano, and Kokotović (1995b) showed that the controller must have a gain that dominated the slope $g_m = \partial \Psi_c / \partial m$ of the compressor characteristic.
- When using a close coupled valve (CCV) to stabilize a centrifugal compressor, the control law gain must be greater than $g_m = \partial \Psi_c / \partial m$, as shown in Gravdahl and Egeland (1999a).

Remark 2. The CCV-approach, as introduced by Simon and Valavani (1991), aims at using the pressure drop over a valve to create a combined compressor and valve characteristic with negative slope in the equilibrium and thereby ensuring stability. It should be noted that the approach in this study achieves the same effect as the CCV approach without imposing an unwanted pressure drop in the compression system. The proposed controller ensures that in closed loop the compressor characteristic has a negative slope in the equilibrium which can be seen from the plot of $\hat{\Psi}_c(\hat{m}, -c\hat{m})$ in Fig. 6.

We now take the shaft dynamics (5c) into consideration in order to investigate the effect on the stability properties of the system. Following the same procedure as in the proof of Theorem 1, the time derivative of the Lyapunov function candidate (15) along the trajectories of (6) is

$$\dot{V} < -k_p \hat{p}^2 - k_m \hat{m}^2 + \hat{m}\delta(t), \tag{22}$$

where

$$\delta(t) = \frac{A}{L} \tilde{\Psi}_c(t)$$

and

$$\tilde{\Psi}_c := \Psi_c(m, \omega) - \Psi_c(m, \omega_d) \tag{23}$$

is the error in the compressor pressure rise Ψ_c due to the shaft dynamics related to the convergence of ω to the desired value $\omega_d = \omega_0 - c\hat{m}$. It is seen from (22) that the system will converge towards a set $\mathscr{A}_1$, which will soon be defined, whenever

$$k_m |\hat{m}| > |\delta(t)|. \tag{24}$$

The set $\mathscr{A}_1$ can be found by using Young's inequality on the last term in (22) which gives

$$\hat{m}\delta(t) < v_1 \hat{m}^2 + \frac{\delta^2(t)}{4v_1} < v_1 \hat{m}^2 + \frac{\|\delta\|_\infty^2}{4v_1}, \quad \forall v_1 > 0, \tag{25}$$

where v_1 is a constant. Consequently, (22) can be written

$$\begin{aligned} \dot{V} &< -k_p \hat{p}^2 - (k_m - v_1)\hat{m}^2 + \frac{\|\delta\|_\infty^2}{4v_1} \\ &= -W(\hat{x}) + \frac{\|\delta\|_\infty^2}{4v_1}, \end{aligned} \tag{26}$$

where $\hat{x} = (\hat{m}\ \hat{p})^\top$, $W(\hat{x}) = \hat{x}^T Q \hat{x}$ and Q is a diagonal matrix given by $Q = diag\{k_p, k_m - v_1\}$. The function $W(\hat{x})$ is positive definite and radially unbounded provided the freely chosen v_1 is selected such that $v_1 < k_m$. As $V(\hat{x})$ and $W(\hat{x})$ defined in (15) and (26) are quadratic, positive definite, radially unbounded and smooth there exist quadratic bounds such that

$$\beta_1 \|\hat{x}\|^2 \leqslant V(\hat{x}) \leqslant \beta_2 \|\hat{x}\|^2 \tag{27}$$

$$\beta_3 \|\hat{x}\|^2 \leqslant W(\hat{x}), \tag{28}$$

where β_1, β_2 and β_3 are positive constants. From (15) it is seen that $V = \hat{x}^T P \hat{x}$, where P is the positive definite diagonal

matrix $P = diag\{V_p/2a_{01}^2, L/2A\}$. Hence, β_1 and β_2 are given by $\beta_1 = \underline{\lambda}_P$ and $\beta_2 = \bar{\lambda}_P$, where $\bar{\lambda}_P = \max\{V_p/2a_{01}^2, L/2A\}$ and $\underline{\lambda}_P = \min\{V_p/2a_{01}^2, L/2A\}$ are the upper and lower eigenvalue of P. The constant $\beta_3 = \underline{\lambda}_Q$, where $\underline{\lambda}_Q = \min\{k_p, (k_m - v_1)\}$ is found from (26) in a similar manner. It now follows from (15), (26), (27) and (28) that $\hat{x}(t)$ is globally uniformly bounded and converges to the compact set

$$\mathscr{A}_1 = \left\{ \hat{x} : \|\hat{x}\| < \sqrt{\frac{(\beta_2/\beta_3)(\|\delta\|_\infty^2/4v_1)}{\beta_1}} \right\}$$

$$= \left\{ \hat{x} : \|\hat{x}\| < \frac{1}{2}\sqrt{\frac{\beta_2}{\beta_1\beta_3 v_1}}\|\delta\|_\infty \right\}. \tag{29}$$

The compactness of $\mathscr{A}_1$ follows from the fact that the bounds in (27) and (28) are quadratic, as is discussed on p. 214 in Khalil (1996). The rate of convergence can be determined as follows. Consider the signal

$$s \triangleq V(\hat{x})e^{\gamma t},$$

where $\gamma > 0$ is a constant. By using (26),(27) and (28), the time derivative of s can be upper bounded as

$$\frac{ds}{dt} = (\dot{V} + \gamma V)e^{\gamma t}$$

$$\leqslant \left(-W(\hat{x}) + \frac{\|\delta\|_\infty^2}{4v_1} + \gamma V\right) e^{\gamma t}$$

$$\leqslant (-\beta_3\|\hat{x}\|^2 + \gamma\beta_2\|\hat{x}\|^2)e^{\gamma t} + \frac{\|\delta\|_\infty^2}{4v_1}e^{\gamma t}.$$

Now, chose γ as

$$\gamma = \frac{\beta_3}{\beta_2},$$

so that

$$\frac{ds}{dt} \leqslant \frac{\|\delta\|_\infty^2}{4v_1}e^{\gamma t}. \tag{30}$$

An upper bound on the state $\hat{x}$ is now found by integrating (30):

$$\int_0^t \frac{ds}{dt'}\,dt' \leqslant \int_0^t \frac{\|\delta\|_\infty^2}{4v_1}e^{\gamma t'}\,dt',$$

$$V(\hat{x}(t))e^{\gamma t} - V(\hat{x}(0)) \leqslant \frac{\|\delta\|_\infty^2}{4\gamma v_1}(e^{\gamma t} - 1),$$

$$V(\hat{x}(t)) \leqslant V(\hat{x}(0))e^{-\gamma t} + \frac{\|\delta\|_\infty^2}{4\gamma v_1}. \tag{31}$$

By using (27), (31), can be rewritten as

$$\underline{\lambda}_P\|\hat{x}(t)\|^2 \leqslant \bar{\lambda}_P\|\hat{x}(0)\|^2 e^{-\gamma t} + \frac{\|\delta\|_\infty^2}{4\gamma v_1},$$

$$\|\hat{x}(t)\| \leqslant \sqrt{\frac{\bar{\lambda}_P}{\underline{\lambda}_P}}\|\hat{x}(0)\|e^{-(\gamma/2)t} + \frac{\|\delta\|_\infty}{2\sqrt{\gamma v_1 \underline{\lambda}_P}},$$

$$\|\hat{x}(t)\| \leqslant \sqrt{\frac{\bar{\lambda}_P}{\underline{\lambda}_P}}\|\hat{x}(0)\|e^{-(\gamma/2)t} + \frac{1}{2}\sqrt{\frac{\beta_2}{\beta_1\beta_3 v_1}}\|\delta\|_\infty, \tag{32}$$

where the fact that $\sqrt{a^2 + b^2} \leqslant |a| + |b|$ has been used. By (32) it follows that $\hat{x}(t)$ converges to $\mathscr{A}_1$ with an exponential rate of convergence given by $\gamma/2 = \beta_3/2\beta_2$.

In the case that the desired speed ω_d is reached, we have the following useful result. Assume that there exists a non-negative monotonically decreasing function $\bar{\delta}(t)$ such that

$$|\delta(t)| < \bar{\delta}(t), \quad \forall t \geqslant 0 \tag{33}$$

and further assume $\omega \to \omega_d$ such that according to (23),

$$\lim_{t\to\infty} \delta(t) = 0. \tag{34}$$

It now follows from an analysis similar to the on p. 77 in Krstić, Kanellakopoulos, and Kokotović (1995a) that in additional to being globally uniformly bounded, $\hat{x}(t)$ converges to the origin.

3.2. Velocity control

Let the electrical motor torque be generated by

$$\tau_d = \hat{\tau} + \tau_0,$$

where

$$\tau_0 = \tau_{c0}$$

is the torque required in the equilibrium point, and

$$\hat{\tau} = K_1(\omega_d - \omega)$$

is the feedback control law that is used to obtain the desired shaft speed

$$\omega_d = \omega_0 - c\hat{m}.$$

The resulting control law is

$$\tau_d = -K_1\hat{\omega} - K_2\hat{m} + \tau_0, \tag{35}$$

where the feedback gain for the mass flow $\hat{m}$ is

$$K_2 = K_1 c.$$

In practical implementations we propose the use of integral action to generate the term τ_0. An integral term

$$\tau_0 = -K_I \int_0^t \hat{\omega}(t')\,dt'$$

is included in order to keep the compressor at the desired speed, and can be regarded as part of the performance control system, see Fig. 1. This results in the control law

$$\tau_d = -K_1\hat{\omega} - K_2\hat{m} - K_I \int_0^t \hat{\omega}(t')\,dt'. \tag{36}$$

By the preceding analysis it follows that applying a drive torque according to (36) ensures that the states of the system (5) converges exponentially to a region around the origin.

3.3. Disturbances

Assume that the compression system is subject to disturbances $\delta_p(t)$ in pressure $\hat{p}$ and $\delta_m(t)$ in mass flow $\hat{m}$ so that the dynamics become

$$\dot{\hat{p}} = \frac{a_{01}^2}{V_p}(\hat{m} - \hat{m}_t) + \delta_p(t), \tag{37}$$

$$\dot{\hat{m}} = \frac{A_1}{L_c}(\hat{\Psi}_c p_{01} - \hat{p}) + \delta_m(t). \tag{38}$$

Under the controller proposed in Theorem 1, the time derivative of the Lyapunov function candidate (15) along the trajectories of (37)–(38) becomes

$$\dot{V} < -k_p\hat{p}^2 - k_m\hat{m}^2 + \hat{p}\delta_p + \hat{m}\delta_m. \tag{39}$$

As the inclusion of disturbances lead to a LFC time derivative of the same structure as (22), an analysis similar to the one in Eqs. (25)–(34) results in the following: The states of the system will be globally ultimately bounded and converge to a compact set

$$\mathscr{A}_2 = \left\{\hat{x} : \|\hat{x}\| < \frac{1}{2}\sqrt{\frac{\beta_2}{\beta_1\beta_4}\left(\frac{\|\delta_p\|_\infty^2}{v_2} + \frac{\|\delta_m\|_\infty^2}{v_3}\right)}\right\}, \tag{40}$$

where the positive constant β_4 is found from the two first terms in (39), and v_2 and v_3 are constants introduced by applying Young's inequality to the last two terms in (39). The set $\mathscr{A}_2$ is found using the same technique leading to the set $\mathscr{A}_1$ in (29). The rate of convergence towards $\mathscr{A}_2$ will be exponential, and if the disturbances satisfy (33) and (34), the states will converge to the origin.

3.4. Torque actuation with disturbances

Including both shaft dynamics and disturbances allow us to combine the above calculations, resulting in an LFC time derivative

$$\dot{V} < -k_p\hat{p}^2 - k_m\hat{m}^2 + \hat{p}\delta_p + \hat{m}\delta_m + \hat{m}\delta(t), \tag{41}$$

from which it can be concluded that controller (35) renders the states of the system (37)–(38) globally ultimately bounded. Exponential convergence to a compact set

$$\mathscr{A}_3 = \left\{\hat{x} : \|\hat{x}\| < \frac{1}{2}\sqrt{\frac{\beta_2}{\beta_1\beta_5}\left(\frac{\|\delta\|_\infty^2}{4v_1} + \frac{\|\delta_p\|_\infty^2}{4v_2} + \frac{\|\delta_m\|_\infty^2}{4v_3}\right)}\right\}, \tag{42}$$

is ensured. The positive constant β_5 is found from the two first terms in (39) using the same technique as before.

4. Implementation issues

4.1. Introducing realistic disturbances

In order to simulate realistic situations, disturbances are introduced in the simulations of the system. Process disturbances in the form of mass flow fluctuations and measurement noise in the mass flow measurement will be considered. The disturbances are of three types:

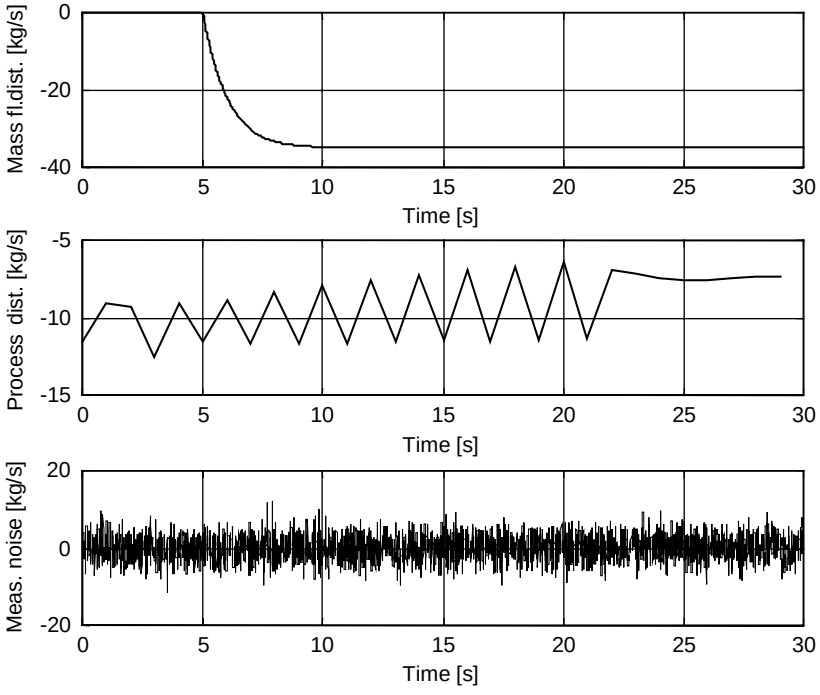

Fig. 7. The different disturbances used in the simulations. From the top: low/medium frequency process disturbances, high-frequency process disturbances and measurement noise.

Low/medium frequency process disturbances: This is larger changes in mass flow due to operational changes for such events as start-up, shutdown, trip of an upstream or downstream compressor, rerouting of gas in a pipeline network, etc. In actual pipeline compressor installations, such disturbances might cause the flow rate to increase/decrease by 10% over a 5-min period. Also, change in consumer demands might cause the flow rate to change in the area of 20%, but over a longer time period. The mass flow drop of 35% that drives the compressor into surge in the simulations in this study takes place at a time scale of 1 s, implemented here as a step which is filtered through a time constant with $T = 1$. The simulated disturbance is chosen to be a worst case version of real world disturbances.

High frequency process disturbances: This is disturbances caused by such phenomena as, e.g. slip relations between the different phases in a multiphase flow. The time series in the middle plot of Fig. 7 is a scaled version of such a disturbance. The mass flow disturbance is taken from simulations of pipeline flow using a multiphase simulator with a sampling interval of 1 s. Again, the disturbance is chosen according to a worst-case scenario.

Measurement noise: The measurement noise is implemented in the simulations as band limited white noise with a power of 0.20 and a sampling interval of 0.010 s. This gives a measurement error in the range of ± 10 kg/s. The measured flow is in the order of 100 kg/s, which implies a measurement error of $\pm 10\%$. This is quite severe when compared to the mass flow measurement shown in the lower plot in Fig. 3 which has a noise level of around $\pm 1.5\%$.

In Fig. 7, the different disturbances that the compressor is experiencing in the simulations are shown. The upper plot is a 35% drop in mass flow driving the compressor into surge. The middle plot is the process disturbances from the pipeline simulations, and the lower plot is the measurement noise.

4.2. Test rig considerations

As of now, plans are being made for a test rig in order to verify the methods in this study experimentally. Different test rig alternatives are being considered, and a number of issues are being studied in connection with this.

Of particular importance is that in a practical implementation the electrical drive will have certain limitations. In the simulations presented in Section 5, these limitations are taken into account. This is implemented in the simulations by using various saturation elements. The limitations include maximum torque, maximum torque rate, maximum speed and maximum acceleration. Numerical values for the saturation limits are given in Appendix A.

When using an electrical drive to actively control surge, it has been found through simulations that the mass flow measurement must be quite fast. In fact, simulations indicate that online measurement of mass flow with a time delay of no more that 50 ms is needed. This calls for a high speed mass flow measurement. On the other hand it is seen in Section 5 that measurement noise is handled well by the controller. Other topics that have been considered, but which is outside the scope of this paper, include vibrations, thermal issues, limitations in the electrical supply grid, hysteresis due to stall and temporary loss of drive power.

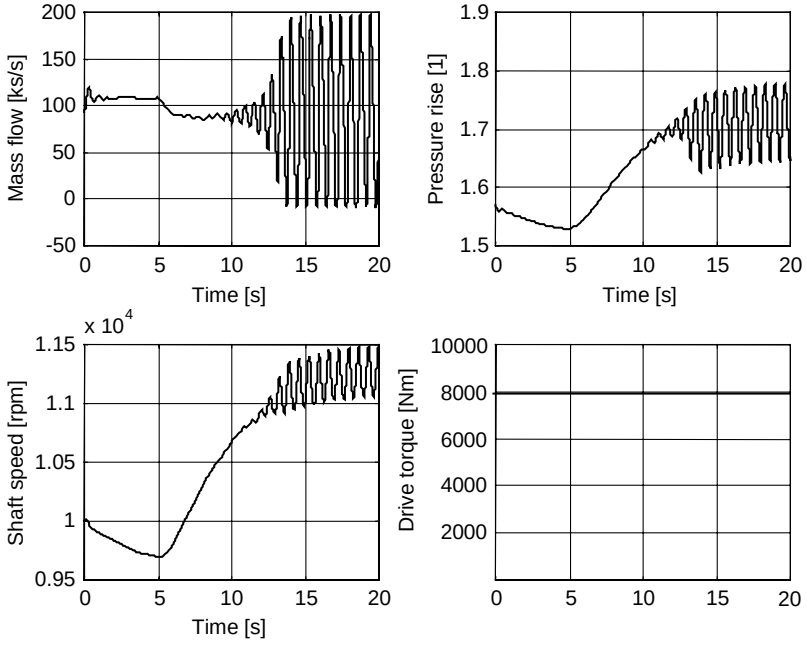

Fig. 8. Compressor response due to 35% drop in mass flow. The system enters surge. The drive torque is kept constant.

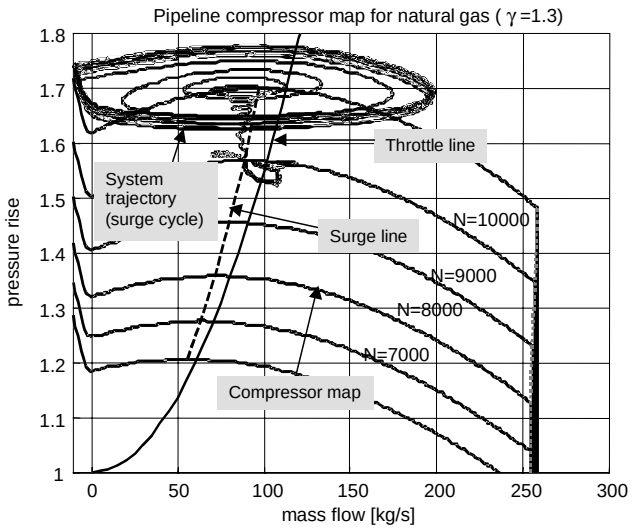

Fig. 9. Surge simulation plotted together with the compressor map. The limit cycle is clearly visible.

5. Simulations

The compressor and electrical drive specified in Appendix A are used in the simulations. This could, e.g. be a compression system for gas transport in pipelines. First, results from simulations of the compressor system when it is driven into surge by a drop in mass flow is presented. The compressor is initially operating in a stable equilibrium at $m \approx 100$ kg/s, when a drop in mass flow of 35% occurs resulting in deep surge. This mass flow drop is shown in the upper plot in Fig. 7, and the compressor response to the disturbance is shown in Fig. 8. A constant drive torque $\tau_d = 8000$ Nm is used. As the operating point crosses the surge line, the compressor undergoes deep surge with oscillations in mass flow, pressure rise and shaft speed. The surge frequency is about 1.6 Hz, which is typical for a compressor of this size. In Fig. 9, the surge cycle is clearly visible on the compressor map. The reason for the higher rotational speed of the compressor during surge is that the drive torque is kept constant during simulation, and as can bee seen from (3) the compressor load torque is lower for this lower mass flow.

So far it has been demonstrated that the compressor becomes unstable when the operating point crosses the surge line. Simulations of the proposed active surge control approach will now be presented. The idea is to control the compressor speed with feedback from the mass flow so that the compressor can operate in a stable mode even to the left of the surge line and thereby avoiding the unstable operation demonstrated in the simulations above. The controller is implemented with the input torque given by (36). The integral term $K_I \int_0^t \hat{\omega}(t')\,dt'$ is included in order to keep the compressor at the desired speed, and can be regarded as part of the performance control system. The following controller gains were used in all the simulations: $K_1 = 10,000$, $K_2 = 500$ and $K_I = 10,000$. Three simulation cases will be presented: 1) The compressor is driven over the surge line by a drop in mass flow, 2) Measurement noise is added and 3) Process disturbances is added.

First, we let the controller (36) is active at all times, and as the drop in mass flow is introduced at $t = 5$ s, the compressor remains stable. This can bee seen in Fig. 10, where the mass flow, pressure rise, shaft speed and drive torque are plotted. As can be seen in Fig. 11, the new and stable operating point is located to the left of the surge line, approximately 20% below the surge line mass flow at this speed, illustrating

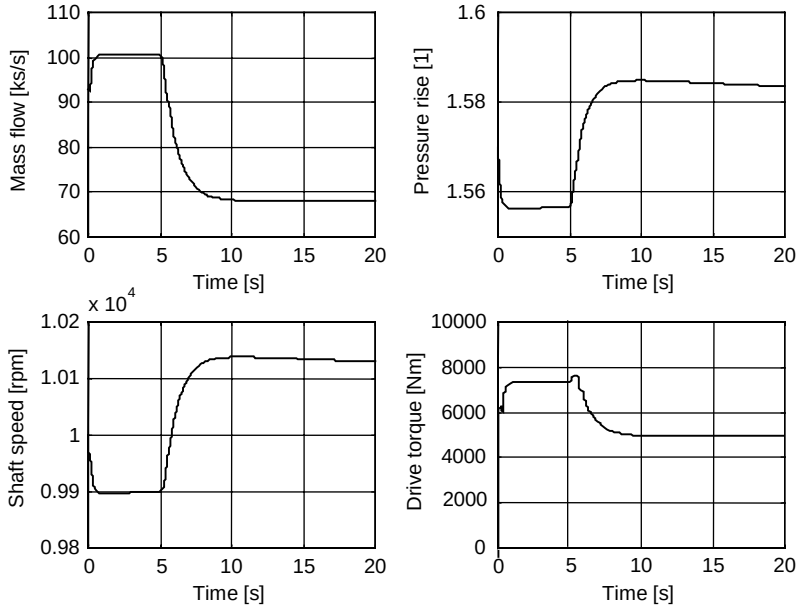

Fig. 10. Stabilization of operating point left of the surge line using the control law (35).

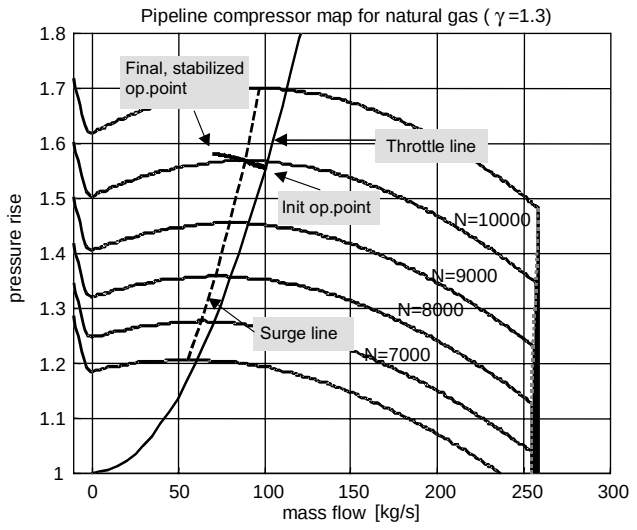

Fig. 11. Same simulation as in Fig. 10 plotted together with the compressor map. The system trajectory crosses the surge line and reaches the stabilized operating point.

the capability of the control system to achieve active surge control.

Then, high frequency measurement noise is taken into account. The noise is shown in the lower plot in Fig. 7, and the resulting simulation is shown in Fig. 12. Due to the measurement noise, the drive torque τ_d, shown in the lower right subplot of Fig. 12, is now quite noisy. However, it is important to stress that the limitations of the drive, specified in Appendix A, is not exceeded. As can be seen, the states of the system remain bounded and converges to a set.

Finally, measurement noise and process disturbances are taken into account. The process disturbance is shown in the middle plot in Fig. 7. As can be seen from the plots in Fig. 13, the controller keeps the compressor stable, and the bounded states converge to a set.

6. Conclusion

In this paper, we have developed a novel active surge controller for centrifugal compressors. By using the electrical drive as actuator and employing feedback from mass flow and rotational speed it has been shown that open loop unstable operating points in the area to the left of the surge line can be made globally exponentially stable. Exponential convergence is ensured in the presence of process disturbances and measurement noise. The results have been confirmed by simulations of a centrifugal pipeline compressor.

Acknowledgements

The authors would like to thank Dr. Michael Schmitz of ABB Turbo Systems AG, Baden, Switzerland for calculating the specifications of the compressor and electrical drive used in the simulations.

Appendix A. Single stage natural gas compressor

The main dimensions of a typical impeller of a single-stage centrifugal compressor have been determined

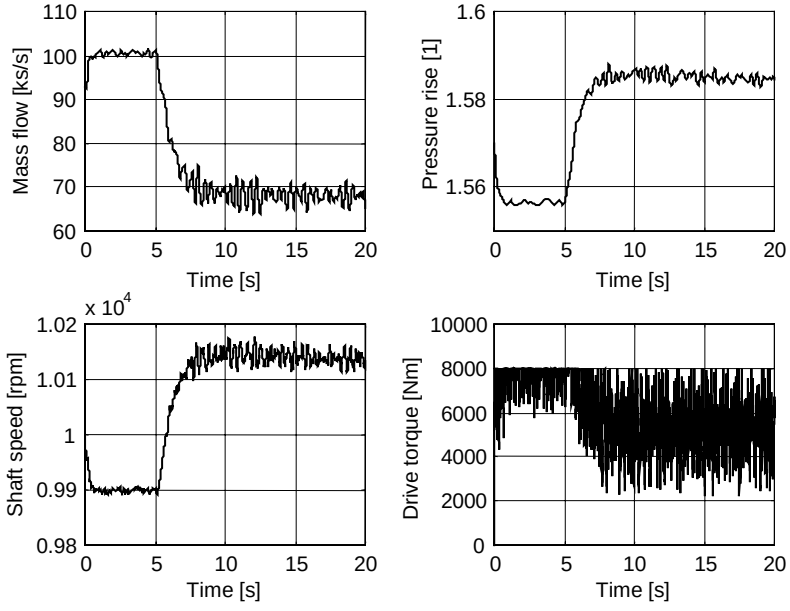

Fig. 12. Same situation as in Fig. 10, with the addition of measurement noise.

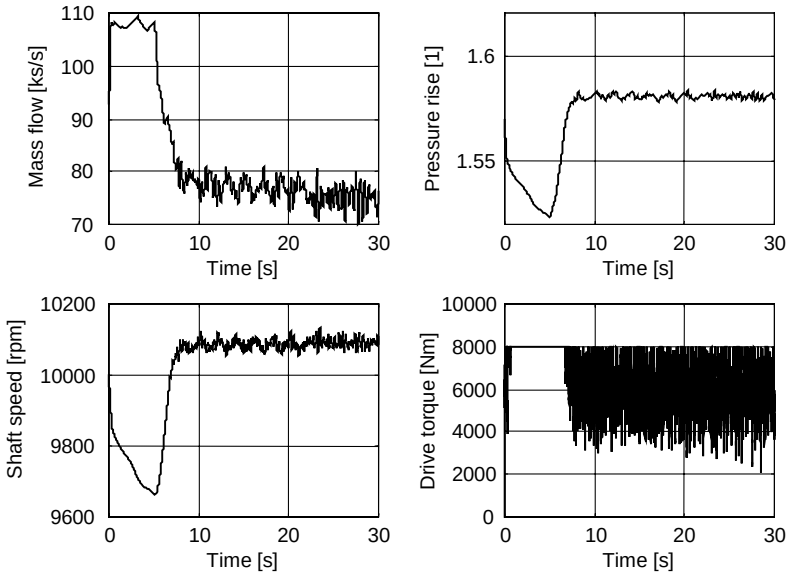

Fig. 13. Same situation as in the ideal case, but now process disturbances and measurement noise is included.

Table 1
Compressor specifications

Outer diameter	$d_2 = 0.557$ m
Inlet diameter (hub)	$d_{h1} = 0.095$ m
Inlet diameter (shroud)	$d_{s1} = 0.210$ m
Blade height at shroud	$b_2 = 8$ mm
No. of blades	$Z = 22$
Blade inlet angle	$\beta_{1b} = 41^\circ$
Moment of inertia	$I_c = 0.9$ kgm^2
Speed	$n = 10,000$ rpm
Power consumption	$P_c = 7.5$ MW
Required torque	$\tau_c = 7100$ Nm

Table 2
Drive specifications

Maximum torque	$\tau_{d,max} = 8000$ Nm
Maximum torque rate	$d\tau_d/dt_{max} = 318320$ Nm/s
Moment of inertia	$I_d = 35$ kgm^2
Maximum speed	$N_{max} = 12000$ rpm
Maximum acceleration	$dN/dt_{max} = 17.4$ 1/s^2

for use in the simulations. The compressor is compressing gas with properties $\kappa = 1.3$ and $c_p = 2064$ J/kg K. The design point is chosen as $m_d = 100$ kg/s, $p_d = 60$ bar, $T_d = 293$ K and $\pi_d = p_{02}/p_{01} = 1.5$. Relevant parameters for the compressor and an actual electrical drive used in the simulations are given in Tables 1 and 2, respectively.

References

Botros, K., & Henderson, J. (1994). Developments in centrifugal compressor surge control–a technology assessment. *Journal of Turbomachinery*, *116*, 240–249.

Cumpsty, N. (1989). *Compressor aerodynamics*. New York: Longman.

de Jager, B. (1995). Rotating stall and surge control: A survey. In *Proceedings of the 35th conference on decision and control*, New Orleans, LA.

Emmons, H., Pearson, C., & Grant, H. (1955). Compressor surge and stall propagation. *Transactions of the ASME*, *77*, 455–469.

Epstein, A., Williams, J. F., & Greitzer, E. (1989). Active suppression of aerodynamic instabilities in turbomachines. *Journal of Propulsion and Power*, *5*(2), 204–211.

Ferguson, T. (1963). *The centrifugal compressor stage*. London: Butterworths.

Fink, D., Cumpsty, N., & Greitzer, E. (1992). Surge dynamics in a free-spool centrifugal compressor system. *Journal of Turbomachinery*, *114*, 321–332.

Gravdahl, J. T., & Egeland, O. (1999a). Centrifugal compressor surge and speed control. *IEEE Transactions on Control Systems Technology*, *7*(5).

Gravdahl, J. T., & Egeland, O. (1999b). *Compressor surge and rotating stall: Modeling and control. Advances in industrial control*. London: Springer.

Gravdahl, J. T., Willems, F., De Jager, B., & Egeland, O. (2000). Modeling for surge control of centrifugal compressors: Comparison with experiment. In *Proceedings of the 39th IEEE conference on decision on control*, Sydney, Australia.

Gravdahl, J. T., Willems, F., de Jager, B., & Egeland, O. (2002). Modeling of surge in variable speed centrifugal compressors: Experimental validation. *Working note*, to be published.

Greitzer, E. (1976). Surge and rotating stall in axial flow compressors, Part I: Theoretical compression system model *Journal of Engineering for Power*, *98*, 190–198.

Greitzer, E. (1981). The stability of pumping systems—The 1980 Freeman scholar lecture. *Journal of Fluids Engineering*, *103*, 193–242.

Khalil, H. (1996). *Nonlinear systems* (2nd ed.). Englewood Cliffs, NJ: Prentice-Hall, Inc.

Krstić, M., Kanellakopoulos, I., & Kokotović, P. (1995a). *Nonlinear and adaptive control design*. New York: Wiley.

Krstić, M., Protz, J., Paduano, J., & Kokotović, P. (1995b). Backstepping designs for jet engine stall and surge control. In *Proceedings of the 35th conference on decision and control*, New Orleans, LA.

Nisenfeld, A. (1982). *Centrifugal compressors*: *Principles of operation and control*. Instrument Society of America.

Simon, J., & Valavani, L. (1991). A Lyapunov based nonlinear control scheme for stabilizing a basic compression system using a close-coupled control valve. In *Proceedings of the 1991 American control conference*.

Staroselsky, N., & Ladin, L. (1979). Improved surge control for centrifugal compressors. *Chemical Engineering* 175–184.

Stodola, A. (1924). *Dampf und Gasturbinen*. Berlin, Sechste auflage: Julius Springer.

Van Essen, H. (1995). *Design of a laboratory gas turbine installation*. Technical report WOC-WET 95.012, Teknische Universteit, Eindhoven.

Whittle, S. F. (1953). *JET. The story of a pioneer*. London: Frederick Muller Ltd.

Willems, F., & De Jager, B. (1999). Modeling and control of compressor flow instabilities. *IEEE Control Systems* 8–18.